A quasiclassical trajectory study of $H+H_2O \rightarrow OH+H_2$: Angular distributions and OH angular momentum alignment

Kimberly S. Bradley and George C. Schatz[a)]
Department of Chemistry, Northwestern University, Evanston, Illinois 60208-3113

(Received 25 November 1997; accepted 11 February 1998)

We present a detailed theoretical study of the $H+H_2O$ reaction dynamics using quasiclassical trajectories and two potential energy surfaces, one from Walch–Dunning–Schatz–Elgersma (WDSE) and one from Isaacson (I5). Collision energies of 1.0, 1.4, and 2.2 eV are considered, and both scalar and vector properties of the product distributions are presented. The vector properties include polarization-dependent differential cross sections (PDDCS) and angular momentum alignment parameters for both OH and H_2. The WDSE and I5 scalar and vector results are in most respects very similar. However, we find that they differ noticeably with respect to angular momentum alignment, with I5 predicting weak OH alignment, while WDSE shows much stronger alignment with the OH angular momentum vector preferentially perpendicular to the scattering plane. The I5 surface is a more recent and more accurate surface for H_3O, so it is extremely encouraging that the alignment predicted by I5 is in quantitative agreement with a recent measurement from Brouard and co-workers. In addition, the I5 differential cross section matches the Brouard results quantitatively, while WDSE does not. Detailed mechanistic information underlying the angular distributions, alignment, and PDDCS results is presented, and we find that the differences between I5 and WDSE alignments are connected to different energy release characteristics of the surface in the corner cutting region. © *1998 American Institute of Physics.* [S0021-9606(98)02119-9]

I. INTRODUCTION

In order to fully understand the dynamics of an elementary reaction such as

$$H+H_2O \rightarrow OH+H_2, \tag{1}$$

it is important to study not only its scalar properties (e.g., how the reaction cross section varies with the energies of the reactants or how the available energy is partitioned among rovibrational states of the products), but also to study its vector properties (e.g., information derived from the directions of the velocity and angular momentum vectors). In recent years, it has become possible to measure many of these vector properties, including differential cross sections, rotational orientation, and alignment parameters, and the correlation between product angular momentum and relative velocity vectors. These measurements raise important questions for theoretical investigation, especially: what do these properties tell us about the reaction dynamics and the potential energy surface which underlies the dynamics, and can we learn more about the potential surface from vector properties than from scalar properties?

The dynamics of reaction (1), its reverse, and their isotopic substituted analogs have been studied by many groups, both experimentally and theoretically, as reviewed recently by Bowman and Schatz.[1] Experiments have been carried out to measure the thermal rate constants,[2–5] to study the effects of translational energy and isotopic substitution on reactive cross sections and energy partitioning,[6–12] and to study the effects of initial vibrational excitation of H_2O and its isotopically substituted counterparts on the reaction dynamics.[13–20] Theoretically, there have been a number of quasiclassical trajectory studies[21–25] and quantum mechanical studies[26–36] in full and reduced dimensionality, and a detailed understanding of the scalar properties of this reaction is now available.

In this paper we examine the vector properties of (1), especially those related to the product OH rotational angular momentum vector, to see if additional information about the reaction dynamics and the underlying potential energy surface can be obtained from newly available measurements that provide such information. Therefore we wish to determine if the product OH molecule of (1) has a rotational angular momentum vector that displays preferential alignment with respect to the scattering plane. If so, we wish to determine if this alignment is the signature of a particular reaction mechanism and of features in the potential surface that give such a mechanism. We also consider vector properties associated with the product H_2 molecule, but because the OH molecule is more amenable to experimental study, our focus will be on OH.

Our work is based on quasiclassical trajectory calculations performed using two previously developed, full-dimensional potential energy surfaces. One of these is an old surface developed by Walch, Dunning, Schatz, and Elgersma (which we denote WDSE)[37,38] that has been used in numerous dynamics studies over the years, but which is known to have several deficiencies. The other is a new surface from Isaacson (denoted I5)[39] that is based on higher quality *ab*

a)Author to whom correspondence should be addressed.

TABLE I. Reactant, product, and saddle point properties of the $H+H_2O$ potential energy surface.[a]

		I5[b]	WDSE[c]	*ab initio*[b]	Expt			I5	WDSE	*ab initio*[d]
OH:	r_e	1.87	1.86	1.87	1.83[e]	SP[f]:	r_{OH1}	1.86	1.86	1.86
	ω_e	3696	3623	3696	3738[e]		r_{OH2}	2.49	2.31	2.49
							r_{H2H3}	1.60	1.64	1.61
H_2:	r_e	1.43	1.43	1.43	1.40[e]		θ	97.2	116.7	96.9
	ω_e	4334	4260	4334	4401[e]		α	16.0	−15.8	16.1
							β	0.0	0.0	0.0
H_2O:	r_{OH}	1.84	1.81	1.84	1.81[g]		ω_1	3730	3545	3705
	r_{HH}	2.88	2.86	2.88	2.86[g]		ω_2	2205	1921	2399
	θ	103.1	104.6	103.1	104.5[g]		ω_3	1086	857	1093
	ω_1	3929	3975	3929	3942[g]		ω_4	684	830	684
	ω_2	3811	3865	3811	3832[g]		ω_5	555	572	634
	ω_3	1655	1687	1655	1649[g]		ω_6	1476i	1527i	1448i
Energy:	$H+H_2O$	0.00	0.00							
	$OH+H_2$	0.67	0.66							
	SP	0.93	0.92							

[a]All distances are given in bohr, angles in degrees, frequencies in wave numbers, and energies in eV.
[b]Reference 39.
[c]References 37 and 38.
[d]Reference 50.
[e]Reference 51.
[f]SP=saddle point. Labeling of hydrogens: H3+H2-O-H1. θ is ∠H1-O-H2, α is the supplementary angle of ∠H3-H2-O, and β is the out-of-plane angle.
[g]Reference 52.

initio calculations than WDSE, and uses a more realistic fitting function. We present both scalar and vector properties for each surface so that the strengths and weaknesses of these surfaces in matching experimental data can be examined; however, the focus of our attention is on the calculation of differential cross sections, alignment parameters, and polarization-dependent differential cross sections. In particular, comparison with experimental measurements[9,40,41] is considered to determine which surface is more accurate, and whether angular and rotational alignment information provide more sensitive tests of features of the reaction dynamics than scalar information.

To outline the rest of this paper, Sec. II provides information about the calculations, including details about the potential energy surfaces and calculations of the angular momentum polarization; Sec. III presents our results and discussion; and Sec. IV summarizes our conclusions.

II. CALCULATIONS

A. Potential energy surfaces

As mentioned previously, two different potential surfaces have been used in this work: WDSE[37–38] and I5.[39] The WDSE surface is an empirical fit to the *ab initio* calculations of Walch and Dunning.[38] In the past it has been successfully used to study the dynamics of the $H+H_2O$ and $OH+H_2$ reactions, despite several known defects.[24] One of these defects is the fact that only one of the H atoms in the water molecule is capable of reacting with the incident H, which makes the cross sections for $H+H_2O$ smaller than they should be by a factor of two. Therefore, to correct for this defect, we have multiplied the WDSE reactive cross sections by two, as has been done in previous studies.[21,22,24] The I5 surface is a fit to *ab initio* results from Kraka and Dunning[42] in the vicinity of the reaction path for $OH+H_2 \rightarrow H+H_2O$, the reverse of (1). It is similar to Isaacson's surface 4,[43] and thus consists of two valence bond three-body terms, together with some additional terms involving the curvilinear bending and torsional coordinates. The I5 surface, although allowing for reaction with either H of H_2O, does not treat the H atoms equivalently. As a result, the two reaction pathways that lead from $H+H_2O$ to $OH+H_2$ [i.e., $H(3)+H(2)-O-H(1) \rightarrow H(3)-H(2)+O-H(1)$ and $H(3)+H(1)-O-H(2) \rightarrow H(3)-H(1)+O-H(2)$] have different barriers. Therefore, in our trajectory calculations we have analyzed only those reactive trajectories associated with the proper barrier, and then the resulting cross sections were multiplied by two.

A comparison of the stationary points of these two potential surfaces, together with experimental and *ab initio* values, is presented in Table I. For the reactants and products, the two surfaces are very similar, and they are in good agreement with the *ab initio* calculations and the experimental values. For the saddle point, the I5 and WDSE geometries are similar, but the frequencies show some differences, with the I5 frequencies closer to the *ab initio* values than WDSE.

B. Trajectory calculations

The $H+H_2O$ dynamics was simulated using a quasiclassical trajectory (QCT) method that has been described elsewhere.[44] Parameters defining the initial conditions are similar to those used previously,[24] with a maximum impact parameter of $b_{max}=4.0\ a_0$ used for both surfaces. For the present simulations, we have integrated 120 000–400 000 trajectories on each potential energy surface, at initial energies of 1.0 (slightly greater than the barrier height), 1.4, and 2.2 eV (the latter two energies being where there are experimental alignment data). All trajectory results in this paper have been analyzed subject to a zero point energy constraint on H_2, so that all trajectories in which the product H_2 mol-

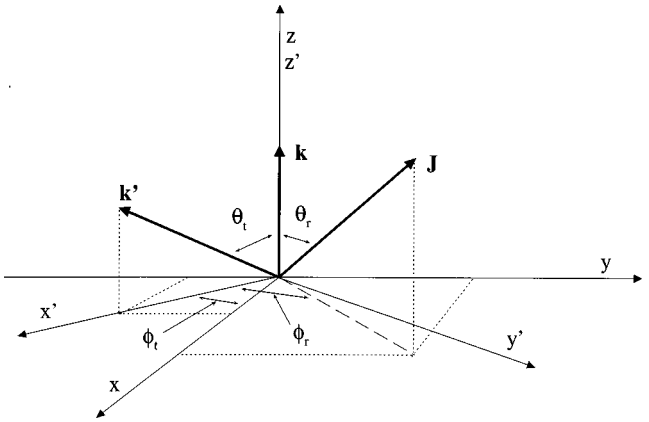

FIG. 1. Diagram illustrating vectors and angles involved in calculations, with symbols defined as in text.

ecule has less than zero point energy are rejected. We have not similarly constrained the OH product zero point energy, since OH is considered to be a spectator mode during reaction. (See Ref. 25 for further discussion). We should note that none of the vector properties that we consider is sensitive to the imposition of zero point energy constraints.

C. Rotational angular momentum polarization distribution calculations

Details of the calculation of the product rotational angular momentum polarization distributions have been presented previously,[45] so we will provide only a brief review here. Figure 1 illustrates the vectors and angles involved in the calculation, where (x,y,z)label the reagent coordinate axes; (x',y',z')label the product coordinate axes; $\mathbf{k}$ is the relative velocity vector of the reagents (which we use to define the z and z' axes); $\mathbf{k}'$ is the relative velocity vector of the products (and we define the $x'z'$ plane to contain $\mathbf{k}'$); $\mathbf{J}$ is the rotational angular momentum vector of the diatomic product [could refer to either OH (where we ignore electronic angular momentum) or H_2]; θ_t is the scattering angle (the angle between the outgoing OH velocity vector and the incoming H atom velocity vector); ϕ_t is the angle between the reagent coordinate x axis and the product coordinate x' axis (this angle is not coupled to the interaction potential, and has a completely random probability distribution, so it can be ignored); θ_r is the angle between the reagent coordinate z axis and $\mathbf{J}$; and ϕ_r is the azimuthal angle associated with the product coordinate x' axis and $\mathbf{J}$.

The full three-dimensional angular distribution associated with $\mathbf{k}$, $\mathbf{k}'$, and $\mathbf{J}$ can be represented by a set of generalized polarization-dependent differential cross sections[46] (PDDCS), $(2\pi/\sigma)(d\sigma_{kq}/d\omega_t)$, where the subscript kq indicates the order of the polarization of the product scattered into the solid angle $d\omega_t$ associated with θ_t and ϕ_t. The PDDCS with $k=q=0$ is the usual differential cross section. Note that in Ref. 46 the PDDCS's are defined in the stationary target frame (the z axis is defined parallel to the product velocity in the laboratory system), but in this paper we use the PDDCS's defined in the scattering frame (the z axis is defined along the direction of $\mathbf{k}$, and the y axis is defined parallel to $\mathbf{k}\times\mathbf{k}'$). QCT calculation of the PDDCS's for $H+H_2O$ follows the method described previously for $H+CO_2$.[45] This method involves weighting reactive trajectories, sorting them into bins of cos θ_t, summing, and then normalizing, so that a general expression for the value of the QCT calculated PDDCS's in the ith cos θ_t bin is given by

$$\frac{2\pi}{\sigma}\frac{d\sigma_{kq}^{i}}{d\omega_t}=\frac{n}{2\sigma}\sum_{j}C_{kq}(\theta_r^j,\phi_r^j)W_j,$$

where the summation index j indicates individual reactive trajectories in the ith cos θ_t bin, n is the number of cos θ_t bins, σ is the total reactive cross section, $C_{kq}(\theta_r,\phi_r)$is a modified spherical harmonic,[47] and W_j is a statistical weight factor determined by the initial impact parameter. If the impact parameter b is sampled randomly such that $b_j=r_j b_{\max}$(where r is a random number between zero and one), then $W_j=2r_j\pi b_{\max}^2/N_{\rm tot}$, where $N_{\rm tot}$ is the total number of trajectories.

The PDDCS's can then be used to construct the center-of-mass angular distribution function,[48]

$$P(\theta_t,\omega_r)=\sum_k\sum_q\frac{2k+1}{4\pi}C_{kq}^{*}(\theta_r,\phi_r)\frac{2\pi}{\sigma}\frac{d\sigma_{kq}}{d\omega_t},$$

where ω_r represents the polar coordinates of $\mathbf{J}$, defined with respect to the $\mathbf{k}$–$\mathbf{k}'$ scattering plane, and $C_{kq}^{*}(\theta,\phi)$ is the complex conjugate of a modified spherical harmonic. Integration of $P(\theta_t,\omega_r)$ may be performed over all scattering angles, resulting in the distribution $P(\omega_r)$, or the integration may be limited to strictly forward or strictly backward scattered products in order to investigate the correlation of ω_r with θ_t.

In many experimental studies in which linearly polarized light is used to pump the reagents and probe the products, it is only possible to determine low order even terms $(k=0,2)$ in the sum over k. This means that it is possible to determine if the products are *aligned* but not *oriented*. However, with trajectories one can determine any number of even and odd k's, with the only limitation being that the statistical error becomes more and more significant as k increases. In most of the calculations that we present, we have considered all even and odd k's up to $k=6$. In a few cases, we present results that are limited to $k=0,2$ to facilitate comparison with experiment.

Due to the planar symmetry of the scattering process, the distribution of the product internuclear axes should be invariant to reflection in the $\mathbf{k}$–$\mathbf{k}'$ $(x'z')$ plane. Consequently,[49]

$$P(\theta_t,\omega_r)\equiv P(\theta_t,\theta_r,\phi_r)=P(\theta_t,\pi-\theta_r,\pi-\phi_r),$$

and $(2\pi/\sigma)(d\sigma_{k0}/d\omega_t)=0$ for k odd, $(2\pi/\sigma)\times(d\sigma_{kq^+}/d\omega_t)=0$ for k even and q odd, or k odd and q even; $(2\pi/\sigma)(d\sigma_{kq^-}/d\omega_t)=0$ for k even and q even, or k odd and q odd, where

$$\frac{2\pi}{\sigma}\frac{d\sigma_{kq\pm}}{d\omega_t}=\frac{2\pi}{\sigma}\frac{d\sigma_{kq}}{d\omega_t}\pm\frac{2\pi}{\sigma}\frac{d\sigma_{k-q}}{d\omega_t}.$$

A less detailed way to express the degree of polarization of $\mathbf{J}$ is through the center-of-mass frame orientation and alignment parameters. In this study, we shall be interested in

TABLE II. Cross sections and product energy partitioning for reactive $H+H_2O$ collisions.[a]

	1.0 eV		1.4 eV		2.2 eV		
	I5	WDSE	I5	WDSE	I5	WDSE	Expt[b]
N	400 000	180 000	200 000	120 000	200 000	120 000	
N_r	401	103	818	376	1069	1012	
$\sigma(a_0^2)$	0.058±0.003	0.028±0.003	0.284±0.010	0.177±0.009	0.381±0.012	0.370±0.012	
$\sigma_f(a_0^2)$	0.014(24%)	0.007(23%)	0.136(48%)	0.059(34%)	0.218(57%)	0.203(55%)	
$\sigma_b(a_0^2)$	0.044(76%)	0.021(77%)	0.148(52%)	0.118(66%)	0.163(43%)	0.167(45%)	
F_{trans}	0.56	0.68	0.57	0.64	0.56	0.57	0.65±0.26
H_2 F_{rot}	0.08	0.11	0.11	0.15	0.17	0.20	
H_2 F_{vib}	0.32	0.07	0.30	0.12	0.24	0.15	
OH F_{rot}	0.04	0.13	0.02	0.08	0.02	0.07	0.04±0.01
OH F_{vib}	0.00	0.00	0.00	0.00	0.00	0.00	<0.004

[a]N=total number of trajectories integrated; σ=total reactive cross section (a_0^2); σ_f=reactive cross section for forward scattered products, with percent of total in parentheses; σ_b=reactive cross section for backward scattered products, with percent of total in parentheses; F_{trans}=fraction of available energy going to relative translation of products; H_2 F_{rot}=fraction of available energy going to H_2 rotation; H_2F_{vib}=fraction of available energy going to H_2 vibration; OH F_{rot}=fraction of available energy going to OH rotation; and OH F_{vib}=fraction of available energy going to OH vibration. All results are for $J\geqslant 0$ (i.e., summing over all final **J** of OH).
[b]Reference 9.

the second-rank parameter for alignment, $A_0^{(2)}=2\langle P_2(\mathbf{J}\cdot\mathbf{k})\rangle = \langle 3\cos^2\theta_r - 1\rangle$, where P_2 is the second Legendre polynomial, and the brackets indicate an average over the distribution of **J** about **k**. There are three important limiting values of the alignment parameter: for **J** perpendicular to **k**, $A_0^{(2)}=-1$; for **J** parallel or antiparallel to **k**, $A_0^{(2)}=+2$; and for a completely isotropic distribution of **J** about **k**, $A_0^{(2)}=0$.

As an example, we have simulated the limiting case in which $\mathbf{J}\perp\mathbf{k}$ by integrating trajectories on the WDSE potential surface at 2.2 eV that were constrained to be strictly planar. The resulting angular distribution [i.e., PDDCS(00)] is very similar in appearance to the corresponding three-dimensional angular distribution that we present later, so we omit a discussion of it at this point. In contrast, information pertaining to the direction of the OH angular momentum vector shows the expected behavior for planar collisions (i.e., the alignment parameter $A_0^{(2)}$is exactly -1, and the distribution function $P(\omega_r)$ is strongly peaked at $\theta_r=\phi_r=90°$).

III. RESULTS AND DISCUSSION

Table II presents cross sections and energy partitioning information for reactive $H+H_2O$ collisions at initial relative translational energies of 1.0, 1.4, and 2.2 eV. Included in this table are the total number of trajectories, N; the number of reactive trajectories, N_r; the integral cross section, σ; the cross sections for scattering in the forward and backward hemispheres, σ_f and σ_b; the fractions of the available energy in translation, F_{trans}; and the corresponding fractions in rotation and vibration, F_{rot} and F_{vib}, for each product diatomic. Note that in calculating the fractions for vibration and rotation, the vibrational and rotational actions were rounded off (quantized) before calculating vibrational and rotational energies. This avoids unphysical results that occur if the actions are used directly without rounding due to zero point violation in OH vibration.

The results in Table II show that 1.0 eV is barely above the reactive threshold energy, with a very small cross section, backward scattered products, and most of the available energy showing up in product translational energy. When the reagent translational energy is increased to 1.4 eV, the cross section rises significantly, the angular distributions become broader as more products are forward scattered, and the energy going into product translation is essentially the same. Increasing the energy further to 2.2 eV leads to a slower increase in the cross section, a preference for forward scattering, and only minor changes in the energy partitioning. Note that the OH product gets no vibrational excitation, and very little rotational excitation, as might be expected for a spectator bond. However, the newly formed H_2 diatomic gets modest rotational and vibrational excitation.

Generally the two potential surfaces give similar results, and comparison with experimental values at 2.2 eV is excellent. However, there are important differences between the WDSE and I5 results for some properties. In particular, the WDSE cross sections are noticeably smaller than I5 at the lowest energy, while the I5 surface gives more energy in H_2 vibration and less in H_2 and OH rotation than WDSE. Perhaps the only comparison with experiment at 2.2 eV that distinguishes WDSE from I5 concerns the fraction of energy in OH rotation. Here we find that $F_{\text{rot}}=0.02$ on I5, which is close to the experimental value of 0.04±0.01, while $F_{\text{rot}}=0.07$ on WDSE. One other comparison that can be made is with the recent results of Brouard *et al.*[40] They find $F_{\text{trans}}=0.87\pm0.09$ at 1.4 eV for OH($J=1$), which is a little higher than either of our results of 0.57±0.02 on I5 and 0.62±0.02 on WDSE under the same conditions.

Figure 2 presents the angular distributions [PDDCS(00)] calculated on both surfaces at 1.0 eV with $J\geqslant 0$ (i.e., summing over all final J of OH), at 1.4 with $2\geqslant J\geqslant 0$ and at 2.2 eV with $J\geqslant 0$ and with $J\geqslant 8$. Except for the $J\geqslant 0$ results, the specific ranges of J were selected to match (at least approxi-

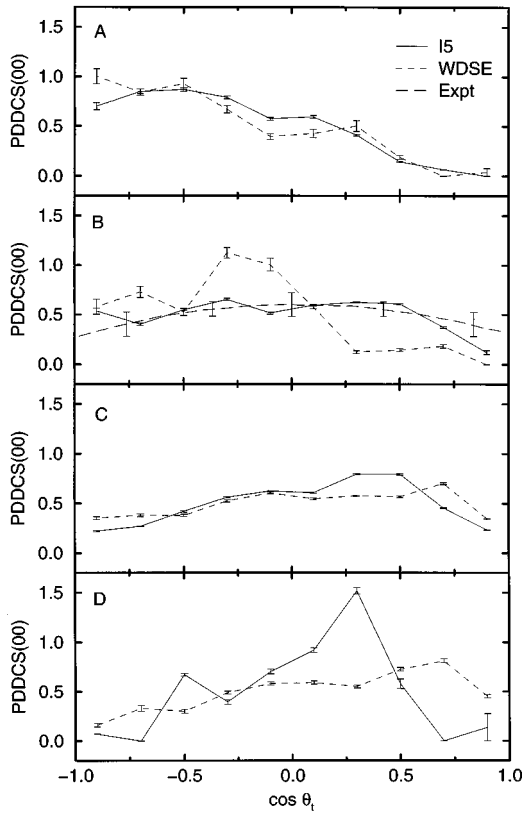

FIG. 2. Angular distribution [PDDCS(00)] as a function of cos θ_t for the I5 and WDSE surfaces at 1.0 eV with $J \geqslant 0$ (A); 1.4 eV with $2 \geqslant J \geqslant 0$ (B); 2.2 eV with $J \geqslant 0$ (C); and 2.2 eV with $J \geqslant 8$ (D).

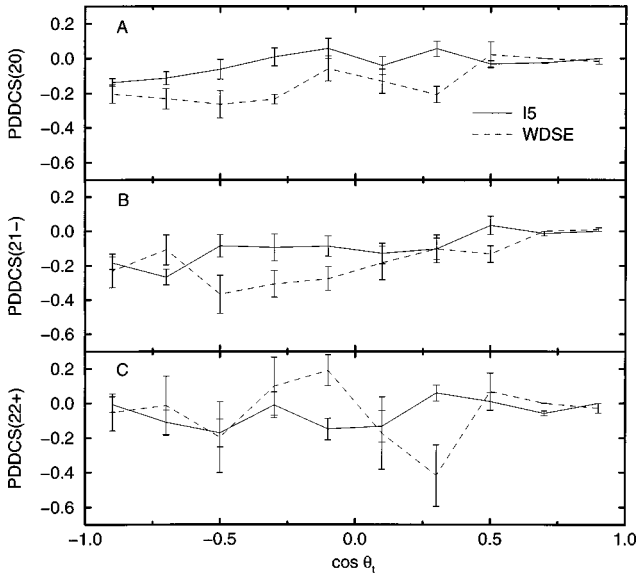

FIG. 3. PDDCS's as a function of cos θ_t for the I5 and WDSE surfaces at 1.0 eV with $J \geqslant 0$. (A) PDDCS(20). (B) PDDCS(21−). (C) PDDCS(22+).

mately) with what has been considered in experiment. As previously noted in our discussion of Table II, the 1.0 eV results on both surfaces show a preference for backward scattering, while for 2.2 eV with $J \geqslant 0$, the distribution is quite broad, with significant forward and backward scattering. Limiting the reactive trajectories to $J \geqslant 8$ yields a preference for the forward scattered products.

At 1.4 eV, the PDDCS(00) shows a preference for backward scattering on WDSE, and is nearly symmetric on I5 (i.e., there is a small backward peak, but σ_f and σ_b are nearly identical). Included in Fig. 2(b) is a comparison with very recent results from Brouard and co-workers.[40] The agreement with I5 is excellent, and it is clearly better than with WDSE. This provides an important test of the relative quality of these two surfaces that will be studied in greater detail later.

Figures 3–5 present PDDCS(20), PDDCS(21−), and PDDCS(22+) for the product OH and translational energies of 1.0 (Fig. 3), 1.4 (Fig. 4), and 2.2 eV (Fig. 5). Note that for Figs. 3 and 4, the results have been summed over all J (i.e., $J \geqslant 0$), while for Fig. 5 we have made the restriction $J \geqslant 8$ (to facilitate comparison with experiment). These figures show that for either surface and at all three energies, the PDDCs's are generally smooth functions of θ_t. The PDDCS(20)'s are all negative for backward scattered products, and gradually increase with cos θ_t to approximately zero for forward scattered products. The other PDDCs's are also negative over much of the range of θ_t. Overall, the results from both surfaces show the same general trends, although there are some quantitative differences that are important. Note especially that at 1.0 eV, and to a lesser extent at 1.4 eV, the WDSE PDDCS(20) is much more negative than I5 for all but the forward direction. This indicates that the WDSE results are more strongly aligned. At 2.2 eV with $J \geqslant 8$, both potential surfaces give very similar results, with the largest difference being in the PDDCS(22+), where the I5 curve shows significant oscillations relative to the WDSE result.

Figures 6 and 7 present the angular distribution functions constructed using the PDDCS's for both surfaces at 1.0 with $J \geqslant 0$, and at 2.2 eV with $J \geqslant 8$. All the PDDCS's with $k = 0$–6 are included in making these plots, and a consistent vertical

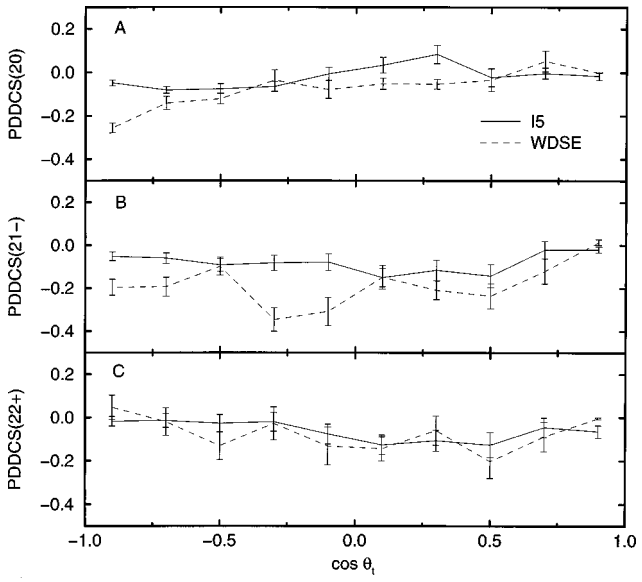

FIG. 4. PDDCS's as a function of cos θ_t for the I5 and WDSE surfaces at 1.4 eV with $J \geqslant 0$ (A) PDDCS(20). (B) PDDCS(21−). (C) PDDCS(22+).

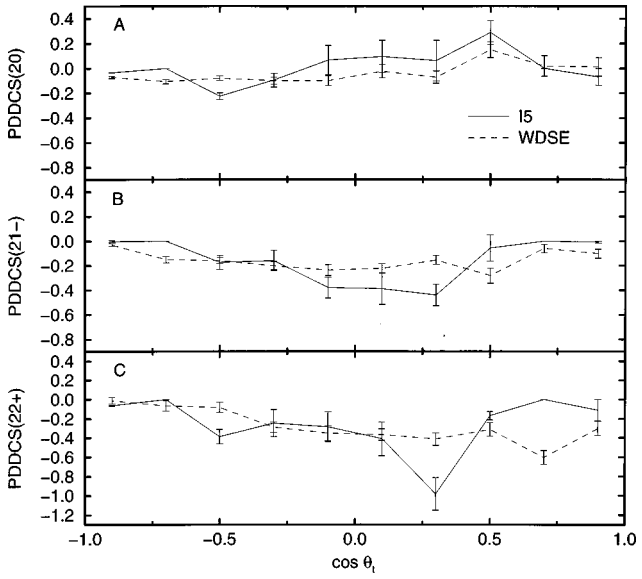

FIG. 5. PDDCS's as a function of cos θ_t for the I5 and WDSE surfaces at 2.2 eV with $J \geq 8$ (A) PDDCS(20). (B) PDDCS(21−). (C) PDDCS(22+).

scale has been used in all plots so that the relative size of the peaks can be compared. Figure 8 presents the corresponding results for the I5 surface at 1.4 eV with $J \geq 0$, comparing angular distributions that include $k=0,2$ to those for $k=0$–6. In Fig. 6, the angular distribution is plotted with integration over *all* reactive trajectories (panels A and B), and with integration over strictly *forward* (panels C and D) or strictly *backward* (panels E and F) scattered trajectories. Figures 7 and 8 refer only to *all* reactive trajectories (panels A and B).

For 1.0 eV with $J \geq 0$ and integration over all trajectories, the distributions from both surfaces [Figs. 6(a) and 6(b)] show a peak in the region of $\theta_r \approx \phi_r \approx 90°$, with the I5 surface [Fig. 6(a)] giving a small ridge and the WDSE surface [Fig. 6(b)] giving a more centralized peak. Limiting integration to strictly forward scattering [Figs. 6(c) and 6(d)], the I5 peak near $\theta_r \approx \phi_r \approx 90°$ is barely above the background oscillations that cover the entire plot, while the WDSE result has a very pronounced peak corresponding to **J** perpendicular to the scattering plane. The strictly backward scattering results on both surfaces [Figs. 6(e) and 6(f)] show ridges in

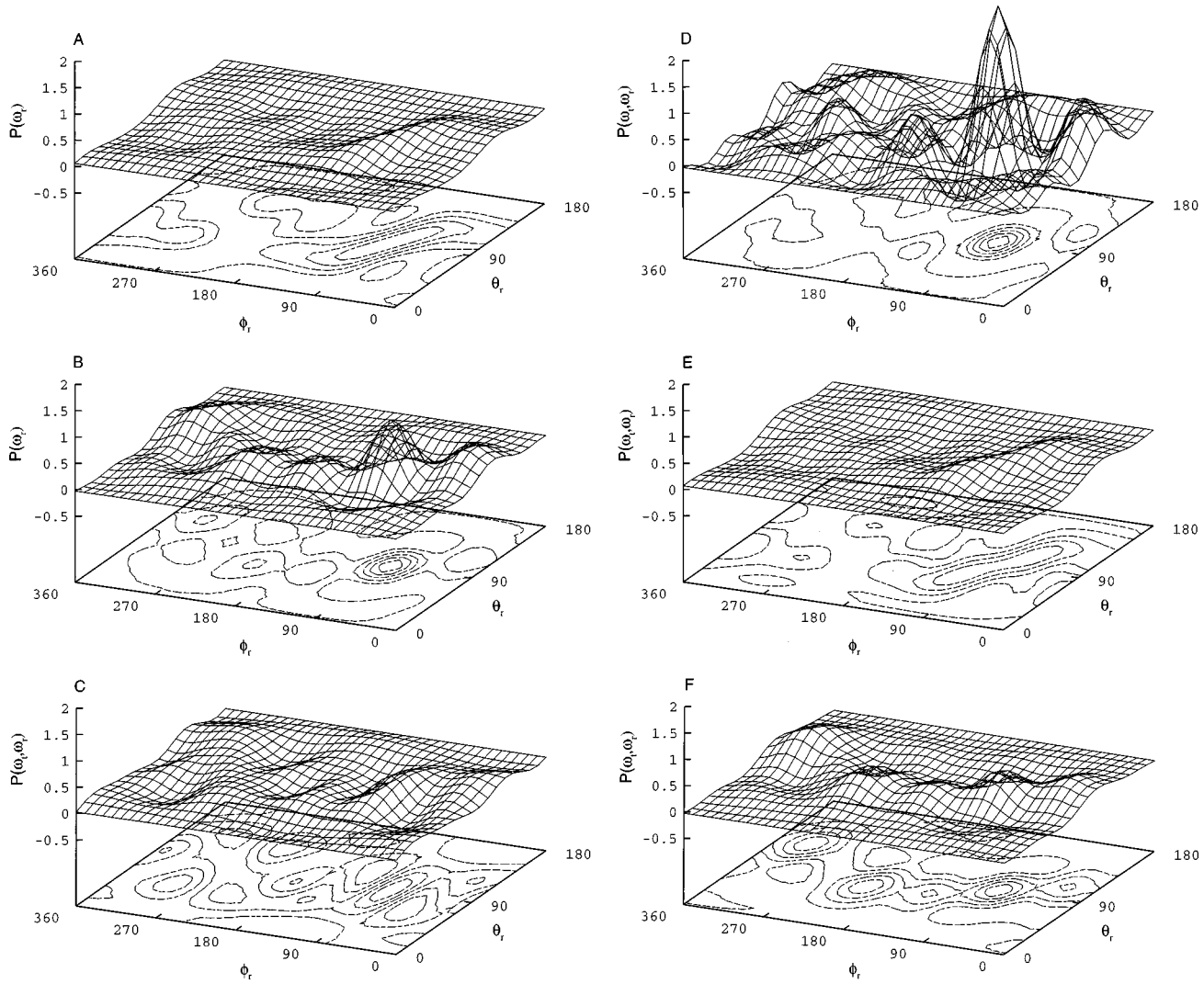

FIG. 6. Angular distribution functions, $P(\omega_r)$ and $P(\omega_t, \omega_r)$ for the I5 and WDSE surfaces at 1.0 eV with $J \geq 0$, and the expansion including terms for $k=0,1,2,3,4,5,6$. (A) I5, integration over all reactive trajectories. (B) WDSE, integration over all reactive trajectories. (C) I5, integration over strictly forward scattered trajectories. (D) WDSE, integration over strictly forward scattered trajectories. (E) I5, integration over strictly backward scattered trajectories. (F) WDSE, integration over strictly backward trajectories.

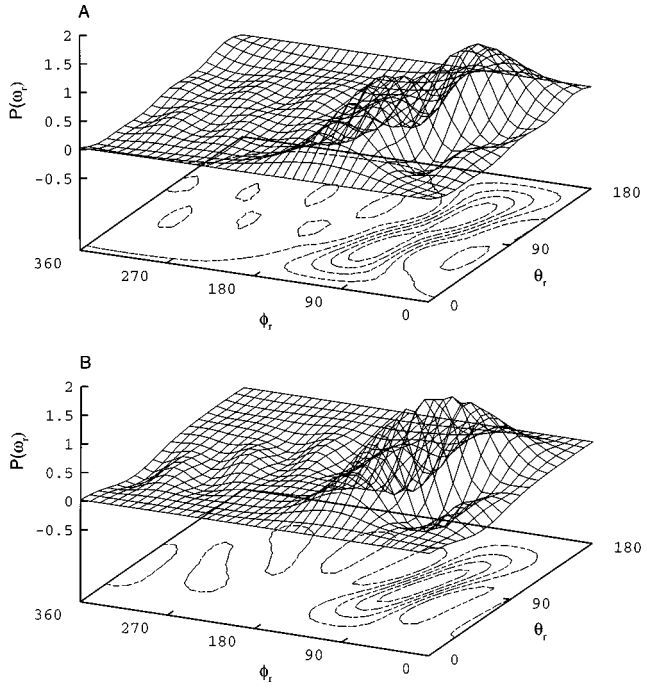

FIG. 7. Angular distribution functions, $P(\omega_r)$ and $P(\omega_t,\omega_r)$, for the I5 and WDSE surfaces at 2.2 eV with $J\geqslant 8$, and the expansion including terms for $k=0,1,2,3,4,5,6$. (A) I5, integration over all reactive trajectories. (B) WDSE, integration over all reactive trajectories.

the region of $\theta_r\approx\phi_r\approx 90°$, with the I5 distribution composed of two small peaks near $\theta_r\approx 45$, $\phi_r\approx 135$, and $\theta_r\approx 135$, $\phi_r\approx 45°$, while the WDSE distribution has a somewhat larger peak centered at $\theta_r=\phi_r=90°$.

For 2.2 eV with $J\geqslant 8$ integration over all trajectories [Figs. 7(a) and 7(b)], the distributions for the two surfaces show ridges centered on $\theta_r\approx\phi_r\approx 90°$ that are closer in appearance to each other than for the corresponding results at 1.0 eV. On the I5 surface, this ridge is divided into twin peaks at $\theta_r\approx 45$, $\phi_r\approx 135$, and $\theta_r\approx 135$, $\phi_r\approx 45°$, while on WDSE, the ridge is somewhat more centralized. The I5 results at 1.4 eV in Fig. 8 that refer to $k=0$–6 [Fig. 8(b)] show behavior somewhat in between the 1.0 and 2.2 eV results. The corresponding results that refer to $k=0,2$ [Fig. 8(a)] show a consistent but much smoother ridge that passes through $\theta_r=\phi_r=90°$, and then is repeated at $\theta_r=90$, $\phi_r=270°$. The repetition that occurs for $\phi_r>180°$ arises from the use of only the even moments. Distributions based on $k=0-6$ show that the ''exact'' distribution is very small for $\phi_r>180°$. This strong asymmetry of the distribution arises because the OH recoils away from the colliding H atom, leading to an angular momentum vector **J** which is significantly oriented parallel to $\mathbf{k}'\times\mathbf{k}$. This means that the product distribution is strongly *oriented*, with PDDCS's for odd k's being as large as the even ones.

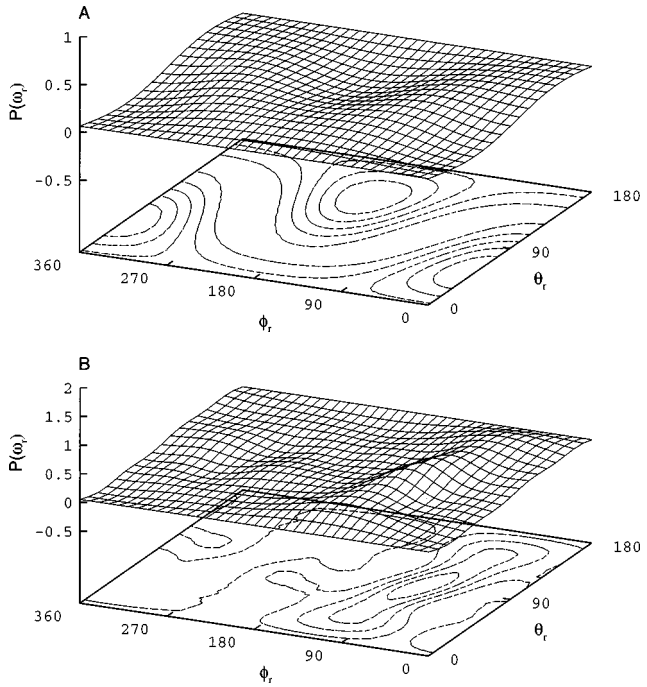

FIG. 8. Angular distribution functions, $P(\omega_r)$, for the I5 surface at 1.4 eV with $J\geqslant 0$ (A) integration over all reactive trajectories and using $k=0,2$, (B) integration over all reactive trajectories and $k=0,1,2,3,4,5,6$.

Table III presents our calculated second-order alignment parameters for both surfaces, including results for both OH and H_2 products. Note that for the 1.4 eV results we consider several different constraints on the OH angular momentum J, including $J\geqslant 0$, $J\geqslant 5$, and $6\geqslant J\geqslant 4$. The last of these is included in order to make comparisons with the experimental data[41] that are available for $J=5$.

Let us consider the OH results in Table III first. At 1.0 eV, the WDSE results for OH show significantly more polarization than do the I5 results, with similar results for forward and backward scattering. For all reactive trajectories, the I5 surface has $A_0^{(2)}=-0.12$, whereas the WDSE surface has $A_0^{(2)}=-0.53$. At 2.2 eV with $J\geqslant 0$, the results for forward and backward scattered products on both surfaces show a similar trend, with the forward scattered products having positive alignment parameters, and the backward scattered products having negative alignment parameters. In all cases, the I5 parameters are more positive than the WDSE parameters, and as a result the sum over all angles gives a negative result on WDSE and a positive result on I5. Similar trends are seen in the 2.2 eV $J\geqslant 8$ results for both surfaces. The 2.2 eV $J\geqslant 8$ alignment parameter can be compared with an experimental result from Jacobs *et al.*[9] for the I5 surface, this value is $+0.04$, which is in reasonable agreement with the WDSE value of -0.15, as both parameters are close to zero. However, these values show significantly less polarization than the experimental value of $-0.94(+0.11, -0.14)$, which is very close to the limit of -1.0 for the strict case where $\mathbf{J}\perp\mathbf{k}$. We have no explanation for this discrepancy; however, the comparison with experiment at 1.4 eV leads to a different conclusion about alignment effects that we now consider.

The calculated OH results at 1.4 eV in Table III are intermediate in nature between those at 1.0 and 2.2 eV, yielding alignment parameters of -0.36 and -0.06 for WDSE and I5, respectively, for $6\geqslant J\geqslant 4$. As expected, the $J\geqslant 0$ results are often more positive than this, and the $J\geqslant 5$ results more negative, but the variation with J is not especially strong. The I5 results are in good agreement with a recent measurement from Brouard,[41] indicating that at least at 1.4 eV the I5 potential surface is preferred, which makes

TABLE III. Second-rank alignment parameters for products OH and H_2.[a]

		I5			WDSE			Expt[b]
		1.0 eV, $J \geqslant 0$	2.2 eV, $J \geqslant 0$	2.2 eV, $J \geqslant 8$	1.0 eV, $J \geqslant 0$	2.2 eV, $J \geqslant 0$	2.2 eV, $J \geqslant 8$	2.2 eV, $J \geqslant 8$
OH	$A_0^{(2)}A$	−0.12	+0.12	+0.04	−0.53	−0.06	−0.15	−0.94(+0.11,−0.14)
	$A_0^{(2)}F$	−0.06	+0.21	+0.24	−0.57	+0.19	+0.06	
	$A_0^{(2)}B$	−0.13	−0.002	−0.31	−0.52	−0.36	−0.48	
H_2	$A_0^{(2)}A$	−0.26	−0.15	−0.32	+0.11	−0.24	−0.26	
	$A_0^{(2)}F$	−0.62	−0.47	−0.56	+0.51	−0.18	−0.31	
	$A_0^{(2)}B$	−0.15	+0.30	+0.09	−0.01	−0.31	−0.18	
		1.4 eV, $J \geqslant 0$	1.4 eV, $4 \leqslant J \leqslant 6$	1.4 eV, $J \geqslant 5$	1.4 eV, $J \geqslant 0$	1.4 eV, $4J \leqslant 6$	1.4 eV, $J \geqslant 5$	1.4 eV, $J=5$[c]
OH	$A_0^{(2)}A$	−0.08	−0.06	−0.24	−0.29	−0.36	−0.39	−0.09
	$A_0^{(2)}F$	+0.06	+0.19	−0.11	−0.10	−0.08	−0.10	
	$A_0^{(2)}B$	−0.22	−0.34	−0.33	−0.38	−0.48	−0.62	
H_2	$A_0^{(2)}A$	−0.28	−0.39	−0.27	+0.06	+0.05	+0.07	
	$A_0^{(2)}F$	−0.57	−0.77	−0.34	+0.10	+0.17	+0.23	
	$A_0^{(2)}B$	+0.02	+0.06	−0.21	+0.04	−0.01	−0.06	

[a] J indicates the magnitude of $\mathbf{J}_{OH}$. A indicates all reactive trajectories were analyzed, whereas F and B indicate that only forward scattered trajectories or only backward scattered trajectories were analyzed, respectively.
[b] Reference 9.
[c] Reference 40.

sense given that it provides a more accurate representation of the true surface. Moreover, the picture that emerges from this comparison is that OH alignment is relatively small unless one examines very high rotational levels of OH for back scattered products.

Let us now consider the H_2 results in Table III. Here we see surprising differences between WDSE and I5 results for forward scattering at 1.0 eV, with I5 giving strongly negative values and WDSE strongly positive. These differences are smaller but still persist at 1.4 eV, whereas at 2.2 eV, all alignments for forward scattering are negative. Note that for the I5 surface, the forward scattered results are consistently more negative than the backward scattered results at all energies, while for WDSE this is true only at the highest energy. To understand these results, we now consider the details of the individual trajectories.

Examination of animated trajectories shows two different reaction mechanisms at work on either surface. The backward scattered products arise primarily from a ''rebound'' mechanism in which the incident hydrogen atom collides nearly collinearly with the H–O bond of the H_2O, and the resulting H_2 is backward scattered. Because of the nearly collinear H–H–O geometry, the transition state is nearly planar, and energy released to the product OH leads to rotational excitation in this plane. As a result, there is preferential OH alignment with $\mathbf{J} \perp \mathbf{k}$. This is responsible for the negative OH alignment parameters seen in the backward direction on both surfaces. The H_2 alignment parameters in the backward direction are mostly negative as well, but only slightly so. This is because the linear H–H–O transition state does not favor H_2 rotation in any particular direction.

Animated trajectories indicate that the forward scattered products arise primarily from a mechanism in which the incident hydrogen atom encounters one of the hydrogen atoms of the H_2O and essentially ''drags'' or pulls it into the forward direction. Nonplanar geometries are more important for this mechanism, and so the forward scattered OH's are more unaligned. However, the dragging process makes the H_2 more strongly aligned. On the I5 surface at all energies, and the WDSE surface at high energies, this dragging leads to frisbee motion of the H_2, and hence negative alignment parameters. Dragging at low energies on WDSE leads to cartwheeling, and hence positive alignments.

To describe the differences between dynamics on I5 and WDSE, we have plotted contours of the two potentials in Fig. 9, as a function of coordinates that correspond approximately to the bond formed and the bond broken during reaction. Also plotted are minimum energy paths for each surface, and two trajectories that refer to forward scattering at 1.0 eV. These plots show that the saddle point geometry is similar on both surfaces, and corresponds to the product region of the $H+H_2O$ reaction. However, there is an important difference in the energy release behavior of the two surfaces going from the saddle point to the reagent region, with I5 showing a more abrupt drop in energy than WDSE (or alternatively one could say the WDSE has more ''repulsive'' energy release than I5). As a result of these differences, the I5 trajectories move smoothly and directly from reagent to productlike motion, while the WDSE trajectories have a harder time turning the corner, resulting in a hard bounce off the inner corner at $R_1=2.4\ a_0$, $R_2=1.7\ a_0$. This bounce produces torsional distortions of the reactive complex and results in cartwheel motion of the H_2 and positive alignment. In contrast, trajectories on the I5 surface have no time for torsional motions, so the planar geometry of the complex is retained throughout the reactive collision. This produces the negative H_2 alignment factors seen on I5.

IV. CONCLUSION

This work has provided much new information about the $H+H_2O$ reaction, especially as pertains to product OH rotational alignment. The most important result is that OH rotational alignment effects and differential cross sections can be

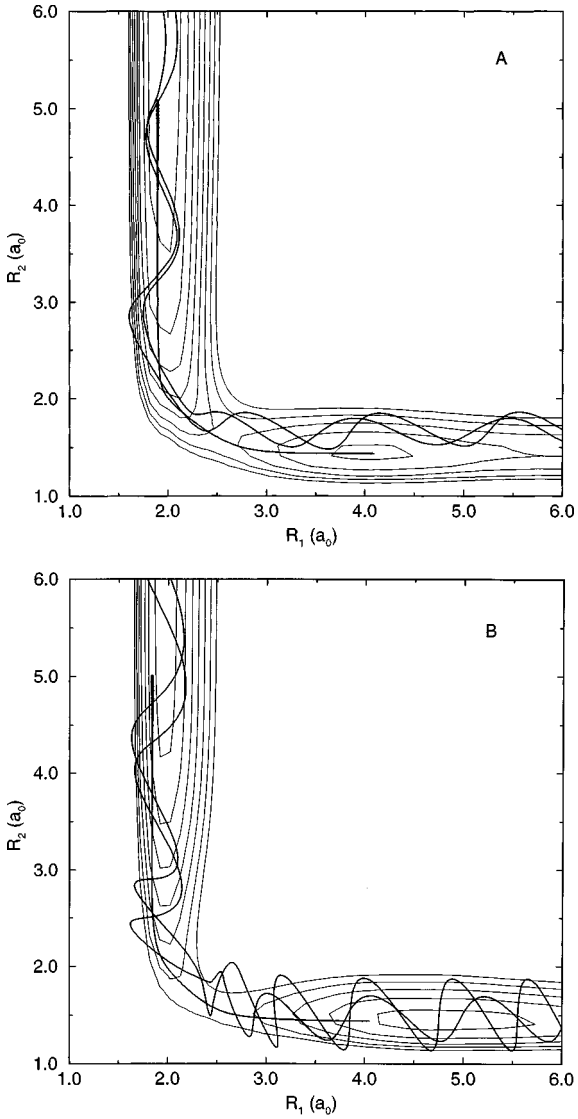

FIG. 9. I5 (A) and WDSE (B) potential energy surfaces, plotted as contours as a function of the distances R_1 and R_2 (in a_0), where for the system H3H2OH1, the H3H2 distance is R_2 and the H2 to OH1 center-of-mass distance is R_1. The potential has been minimized with respect to the other distances and angles with the constraint that they be close to values appropriate for the reaction path. Superimposed onto the contours are two reactive trajectories (1.0 eV translational energy and forward scattered), and the steepest descents path that starts from the saddle point.

used to distinguish the I5 and WDSE surfaces under circumstances where their scalar properties are nearly the same. The excellent agreement of the I5 alignment parameter and differential cross section with experiment is consistent with the idea that this surface provides a better representation of the correct H_3O potential surface. Moreover, we have connected the differences in alignment properties for the two surfaces to trajectory motion and potential energy surface properties.

This paper has also provided a detailed study of the alignment effects for the $H+H_2O$ reaction. For the more reliable I5 surface, we find that OH rotational alignment effects are quite small, indicating that reaction through a range of transition state geometries is possible. In addition, we find that forward scattering (arising from the ''dragging'' mechanism) in particular yields small OH alignment. H_2 alignment is, by contrast, quite strong in forward scattering, primarily through frisbeelike motion that accompanies the dragging mechanism. Backward scattering reverses these trends, with OH alignment becoming much stronger, and H_2 alignment much weaker.

Although the alignment parameters provide a rough indication of the nature of the angular momentum alignment distributions, greater detail is achieved by examining the polarization distribution functions. Here we found significant differences between the nature and shape of the distributions, even when they all exhibited a significant feature at $\theta_r \approx \phi_r \approx 90°$. We look forward to the completion of experimental studies of these distributions so that a higher resolution comparison of theory and experiment can be implemented.

ACKNOWLEDGMENTS

This research was supported by NSF Grant No. CHE-9527677. We thank Alan Isaacson for a copy of the I5 potential surface, as well as Hansi Volpp and Mark Brouard for unpublished data and many valuable discussions.

[1] J. M. Bowman and G. C. Schatz, Annu. Rev. Phys. Chem. **46**, 169 (1995).
[2] C. P. Fenimore and G. W. Jones, J. Phys. Chem. **62**, 693 (1958).
[3] G. Dixon-Lewis, M. M. Sutton, and A. Williams, Trans. Faraday Soc. **61**, 255 (1965).
[4] S. Madronich and W. Felder, J. Phys. Chem. **88**, 1857 (1984).
[5] J. V. Michael and J. W. Sutherland, J. Phys. Chem. **92**, 3853 (1988).
[6] K. Kleinermanns and J. Wolfrum, Appl. Phys. B: Photophys. Laser Chem. **34**, 5 (1984).
[7] A. Jacobs, H.-R. Volpp, and J. Wolfrum, *24th International Symposium on Combustion* (The Combustion Institute, Pittsburgh, PA, 1992).
[8] A. Jacobs, H.-R. Volpp, and J. Wolfrum, Chem. Phys. Lett. **196**, 249 (1992).
[9] A. Jacobs, H.-R. Volpp, and J. Wolfrum, Chem. Phys. Lett. **218**, 51 (1994).
[10] A. Jacobs, H.-R. Volpp, and J. Wolfrum, J. Chem. Phys. **100**, 1936 (1994).
[11] K. Kessler and K. Kleinermanns, Chem. Phys. Lett. **190**, 145 (1992).
[12] K. Honda, M. Takayanagi, T. Nishiya, H. Ohoyama, and I. Hanazaki, Chem. Phys. Lett. **180**, 321 (1991).
[13] A. Sinha, M. C. Hsiao, and F. F. Crim, J. Chem. Phys. **92**, 6333 (1990).
[14] A. Sinha, J. Phys. Chem. **94**, 4391 (1990).
[15] F. F. Crim, M. C. Hsiao, J. L. Scott, A. Sinha, and R. L. van der Wal, Philos. Trans. R. Soc. London, Ser. A **332**, 259 (1990).
[16] A. Sinha, M. C. Hsiao, and F. F. Crim, J. Chem. Phys. **94**, 4928 (1991).
[17] M. C. Hsiao, A. Sinha, and F. F. Crim, J. Phys. Chem. **95**, 8263 (1991).
[18] M. J. Bronikowski, W. R. Simpson, B. Girard, and R. N. Zare, J. Chem. Phys. **95**, 8647 (1991).
[19] M. J. Bronikowski, W. R. Simpson, B. Girard, and R. N. Zare, J. Phys. Chem. **97**, 2194 (1993).
[20] M. J. Bronikowski, W. R. Simpson, B. Girard, and R. N. Zare, J. Phys. Chem. **97**, 2204 (1993).
[21] H. Elgersma and G. C. Schatz, Int. J. Quantum Chem., Quantum Biol. Symp. **15**, 611 (1981).
[22] G. C. Schatz, M. C. Colton, and J. L. Grant, J. Phys. Chem. **88**, 2971 (1984).
[23] K. Kudla and G. C. Schatz, Chem. Phys. Lett. **193**, 507 (1992).
[24] K. Kudla and G. C. Schatz, J. Chem. Phys. **98**, 4644 (1993).
[25] K. Kudla and G. C. Schatz, Chem. Phys. **175**, 71 (1993).
[26] D. C. Clary, J. Chem. Phys. **95**, 7298 (1991).
[27] D. C. Clary, Chem. Phys. Lett. **192**, 34 (1992).
[28] G. Nyman and D. C. Clary, J. Chem. Phys. **99**, 7774 (1993).
[29] D. Wang and J. M. Bowman, Chem. Phys. Lett. **207**, 227 (1993).
[30] J. M. Bowman and D. Wang, J. Chem. Phys. **96**, 7852 (1992).
[31] D. Wang and J. M. Bowman, J. Chem. Phys. **98**, 6235 (1993).
[32] H. Szichman, I. Last, A. Baram, and M. Baer, J. Phys. Chem. **98**, 828 (1994).

[33] H. Szichman and M. Baer, J. Chem. Phys. **101**, 8620 (1994).
[34] H. Szichman and M. Baer, Chem. Phys. Lett. **242**, 285 (1995).
[35] D. H. Zhang and J. C. Light, J. Chem. Phys. **104**, 4544 (1996).
[36] D. H. Zhang and J. C. Light, J. Chem. Phys. **105**, 1291 (1996).
[37] S. P. Walch and T. H. Dunning, J. Chem. Phys. **72**, 1303 (1980).
[38] G. C. Schatz and H. Elgersma, Chem. Phys. Lett. **73**, 21 (1980).
[39] A. D. Isaacson, J. Chem. Phys. **107**, 3832 (1997).
[40] M. Brouad, G. A. J Markillie, K. McGrath, and C. Vallance, Chem. Phys. Lett. **281**, 97 (1997).
[41] M. Brouard (private communication).
[42] E. Kraka and T. H. Dunning, Jr. (unpublished).
[43] A. D. Isaacson, J. Phys. Chem. **96**, 531 (1992).
[44] L. L. Gibson and G. C. Schatz, J. Chem. Phys. **83**, 3433 (1985).
[45] K. S. Bradley and G. C. Schatz, J. Chem. Phys. **106**, 8464 (1997).
[46] N. E. Shafer-Ray, A. J. Orr-Ewing, and R. N. Zare, J. Phys. Chem. **99**, 7591 (1995).
[47] R. N. Zare, *Angular Momentum* (Wiley, New York, 1988).
[48] M. Brouard, H. M. Lambert, S. P. Rayner, and J. P. Simons, Mol. Phys. **89**, 403 (1996).
[49] F. J. Aoiz, M. Brouard, and P. A. Enriquez, J. Chem. Phys. **105**, 4964 (1996).
[50] A. D. Isaacson and S.-C. Hung, J. Chem. Phys. **101**, 3928 (1994).
[51] K. P. Huber and G. Herzberg, *Constants of Diatomic Molecules* (Van Nostrand Reinhold, New York, 1979).
[52] A. R. Hoy, I. M. Mills, and G. Strey, Mol. Phys. **24**, 1265 (1972).